Development of a low-Q cavity-type beam position monitoring system

S. W. Jang, E.-S. Kim*, A. Heo, Y. Honda, T. Tauchi, N. Terunuma and J. G. Hwang

***Abstract*—A beam position monitor (BPM) with nanometer-scale position resolution and decay time of approximately 20 ns is developed as an interaction point (IP) beam position monitor, to verify the nanometer stabilization of the International Linear Collider beam trains at the Accelerator Test Facility (ATF), High Energy Accelerator Research Organization (KEK). The developed low-Q cavity BPM consists of a one-cell sensor cavity and a one-cell reference cavity. An electronic system is developed, based on the beam test results, to process the signals from the BPM. The beam position resolution of the low-Q cavity BPM with the electronics system is measured at the ATF2 beam line of KEK, and the results of the beam tests conducted on the developed low-Q cavity-type BPM are described.**

***Index Terms*—Cavity BPM, ATF2, KEK, Beam Position Monitor, Resolution, ILC.**

I. Introduction

The International Linear Collider (ILC) [1] is a next-generation accelerator designed to address some of the important questions in our universe. The ILC is a 250 to 500 GeV center-of-mass high-luminosity linear electron–positron collider based on 1.3 GHz superconducting radio-frequency (SCRF) accelerating cavities. The ILC allows beam focusing down to a few nanometers at the interaction point (IP). In addition to being focused sharply, the beam for the proposed ILC has to be controlled very precisely. For precise beam-orbit control at the IP, fast beam-based feedback systems [2] and very precise beam position monitors (BPMs) [3] are required; these feedback systems must operate within nanosecond time scales and the BPMs should be able to measure nanometer-level position resolutions. Because a low-emittance beam is produced, and is available at ATF in KEK, the ATF is an ideal facility to develop instrumentation for the ILC, including a high-resolution BPM. The ILC and ATF2 design parameters are compared in Table I.

TABLE I
ILC Technical Design Report and ATF2 parameters.

Parameter	ILC	ATF2
Beam energy (GeV)	250/500	1.3
Number of e^- per bunch (N)	2×10^{10}	1×10^{10}
Bunch interval (ns)	554	$150 \sim 300$
Bunch number	1321	60
Norm. emittance ε_x (m)	1×10^{-5}	3×10^{-6}
Norm. emittance ε_y (m)	3.5×10^{-8}	3×10^{-8}
Beam size σ_x (μm)	0.72/0.47	2
Beam size σ_y (nm)	7.7/5.9	37

The first goal of ATF2 [4] is to achieve a vertical beam size of 37 nm in the IP region and the second goal is to achieve a beam position resolution of 2 nm for the fast beam feedback system to maintain nanometer scale stability for the beam collisions in the IP region. The high-Q cavity-type BPM [5] developed by KEK was tested at the ATF2 exaction beam line and a beam position resolution of 8.7 nm was measured for the Y-port. The decay times of the high-Q BPMs were 59 ns and 30 ns for the x-port and y-port, respectively. The high-Q BPM signal did not decay within 150 ns bunch spacing, and thus, the second bunch overlapped with the tail signals of the first bunch. The fast beam feedback system required a feedback processing time of 100 ns and a BPM signal processing time below 50 ns. The detailed ATF2 layout is shown in Fig. 1. For the fast beam-based feedback system, an improved cavity-

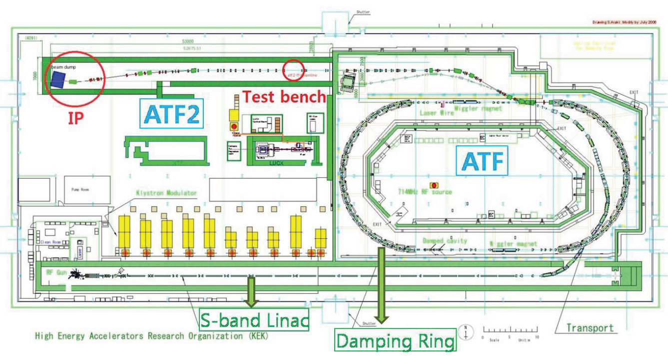

Fig. 1. ATF2 layout, where the ATF2 is the extended test beam line of ATF for the final focus system in a future linear collider.

type BPM with low-Q value and electronics is developed. The major improvement of the new BPM is the increased short-signal decay time of ~20 ns, which helps to distinguish the multibunch signals without signal overlap. To achieve a small loaded Q value for a short decay time, we employ a cavity BPM with a large coupling slot size in the sensor cavity, which

Manuscript received April 12, 2017; revised June 7, 2017; accepted June 8, 2017. This work was supported by the Basic Science Research Program through the National Research Foundation of Korea funded by the Ministry of Education, Science, and Technology under Grant 2011-0016039. (Corresponding author: E.-S. Kim.)

S. W. Jang and E.-S. Kim are with the Accelerator Science Department, Korea University Sejeong Campus, Sejong 339-700, South Korea (e-mail: siwony@korea.ac.kr, eskim1@korea.ac.kr).

A. Heo is with the Physics Department, Kyungpook National University, Daegu, 41566, South Korea.

T. Tauchi and N. Terunuma are with High Energy Accelerator Research Organization (KEK), Tsukuba, 300-3256, Japan.

J. G. Hwang is with Helmholtz-Zentrum Berlin (HZB), Albert-Einstein-straβe 15, 12489 Berlin, Germany.

Color versions of one or more of the figures in this paper are available online at http://ieeexplore.ieee.org.

Digital Object Identifier 10.1109/TNS.2017.2718033

uses stainless steel as the cavity material for a reference cavity. The electronics are also developed so as to reduce the signal processing time to less than 20 ns. The performance of the low-Q BPM system is tested in the ATF extraction line at KEK. In this paper, we describe the cavity BPM principle, the developed low-Q cavity BPM, and the results of the beam tests at ATF2. The characteristics of the developed homodyne electronic system are also presented.

II. Low-Q cavity BPM development

A. Motivation for rectangular-cavity BPM

The limit of the beam position resolution for a strip-line BPM or button-type BPM is approximately 1 μm, which is insufficient to achieve the second goal of ATF2. To obtain a more precise beam position resolution using the BPM, we choose the cavity-type BPM. The usual cavity BPMs use cylindrical shapes, but the cylindrical cavity BPMs provide the same dipole frequencies for the x and y ports. The IPBPM, however, should be capable of measuring much smaller signals in the vertical direction, compared to those in the horizontal direction. Therefore, the isolation of the two dipole modes is of utmost importance for nanometer position resolution. For this reason, we select a rectangular shape to explicitly separate the x and y port frequencies, and thus isolate these two dipole modes perfectly [3], [5].

The final focus system focuses the vertical beam size rapidly; however, such strong focusing optics result in trajectory angle jitters. The angle signal jitter in the vertical direction can contaminate the position information during the position measurements. The cavity length along the beam direction is strongly related to the angle sensitivity; if the cavity length of the BPM is reduced, the angle sensitivity can be reduced. However, the cavity length is also proportional to the stored energy inside cavity; therefore, the cavity length cannot be reduced infinitely. In addition, the small aperture of the beam pipe improves the orbit sensitivity.

The frequencies selected for the x and y dipole modes are 5.712 and 6.426 GHz, respectively. Although there is no global optimal dipole frequency for each BPM application, it is desirable to identify the operating point in the generated dipole mode energy. The generated dipole mode energies for different cavity lengths and frequencies are shown in Fig. 2, along with the points of operating frequency, for the cavity BPM. The generated dipole mode energy is sacrificed to reduce the effects of bunch factor and beam angle. However, the principle resolution determined from the ratio of the calculated dipole mode signal to the thermal noise is below the nanometer range.

B. Design

The Q_0 and resonant frequency are strongly dependent on the cavity material and cavity size. The desired resonant frequencies are 5.712 and 6.426 GHz, and the material is selected as copper. After the stored energy calculation, the cavity length in the Z direction, L, is fixed at 5.8 mm and the rectangular cavity size of the low-Q cavity BPM is determined to be 60.99 mm by 48.59 mm.

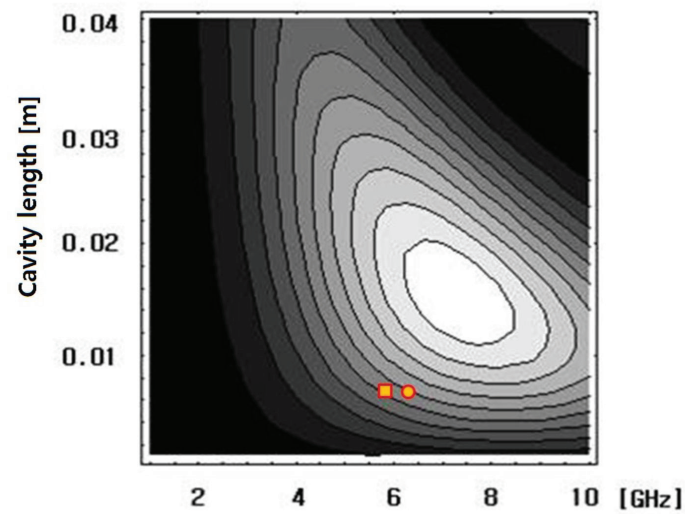

Fig. 2. Generated dipole mode energies for different cavity lengths. The assumed bunch length is 8 mm RMS. The rectangles and circles indicate the x and y dipoles, respectively.

The decay time of the cavity BPM depends on the Q_L value; therefore, the Q_L is a very important parameter for the low-Q IPBPM. As mentioned before in the introduction section, the decay time of a high-Q value IPBPM is not suitable for a fast beam feedback system. The residual leakage of the high-Q IPBPM after a bunch spacing of 150 ns remains at $\sim$28% for the x port. Therefore, we need more complicated analyses for the second beam bunch, and longer signal processing times are required. Therefore, the decay time of the low-Q IPBPM should be lower than that of the high-Q IPBPM. A method to reduce the Q_L for a short decay time is the optimization of the coupling slot size [6], because the coupling slot size determines the Q_{ext} value. If the Q_{ext} value can be reduced through adjustments to the coupling slot size, the Q_L will also be smaller. Equation 1 shows the relation between the quality factors and the decay time τ [7],

$$\tau = \frac{Q_L}{2\pi f} = \frac{Q_0 Q_{ext}}{2\pi f(Q_0 + Q_{ext})}. \tag{1}$$

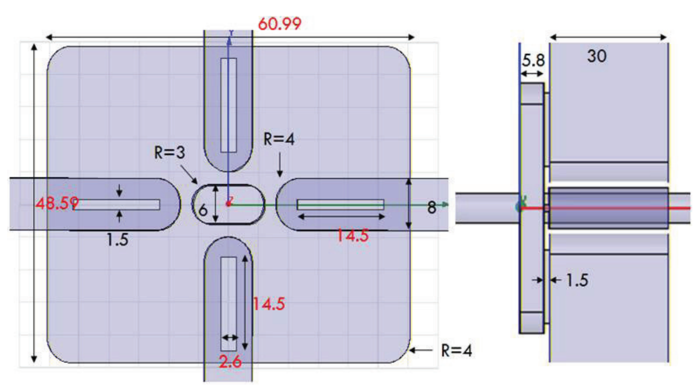

Fig. 3. Dimensions of low-Q cavity BPM. The coupling slot sizes are optimized for a short decay time.

The optimized dimensions for the coupling slots are shown in Fig. 3, and the decay times of the low-Q cavity BPM for x and y dipoles are designed to be 18 ns and 15 ns, respectively. The residual leakage in the cavity BPM, after a bunch spacing of 150 ns for the first bunch, remains below 2% of the peak voltage of $V_{out,0}$ [7].

$$V_{out}(t) = V_{out,0}\ \exp(-\frac{\mathrm{t}}{2\tau})\sin(\omega \mathrm{t} + \phi). \tag{2}$$

TABLE II
LOW-Q CAVITY BPM DESIGN PARAMETERS.

Port	f (GHz)	β	Q_0	Q_{ext}	Q_L	$\tau(ns)$
x	5.712	8	5900	730	650	18.1
y	6.426	9	6020	670	603	14.9

A waveguide is used for the rejection of the monopole mode, so that we can detect a clear dipole mode signal at the feedthrough antenna. The dimensions of the waveguide are designed to satisfy the condition that the cutoff frequency should be located between the x-dipole modes and the monopole mode. The monopole mode frequency is lower than 4 GHz and the x-dipole mode frequency is 5.712 GHz. Through analytical calculations, the waveguide cutoff frequency is set to ∼5 GHz. The excited electrical field is picked up by a feedthrough antenna whose position is optimized using HFSS(High Frequency Structural Simulator) simulation [8]. If the antenna position is optimized ideally, the reflection S parameter (S_{11}) will be zero. Fig. 4 shows the reflection S parameters due to the resonant frequency after antenna position optimization. The optimized low-Q cavity BPM design parameters are listed in Table II.

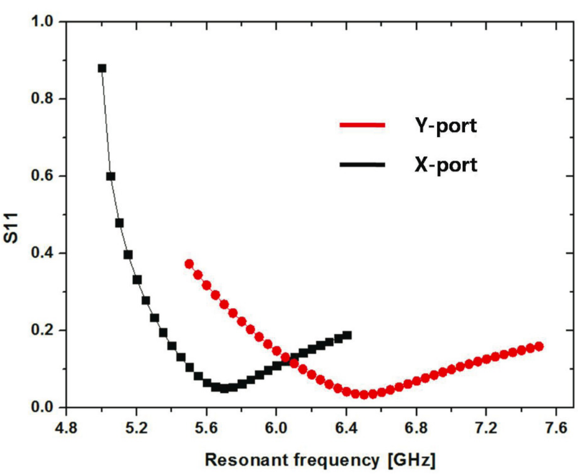

Fig. 4. Reflection S parameters due to resonant frequency after antenna position optimization.

The exchange of energy between the beam and the cavity depends on the geometry of the cavity, rather than on the cavity material, and it can be characterized by the normalized shunt impedance described in Eq. 3.

$$\frac{R}{Q} = \frac{\mid \int \boldsymbol{E}\, ds \mid^2}{P_{wall}} \frac{P_{wall}}{\omega_0 U} = \frac{\mid \int \boldsymbol{E}\, ds \mid^2}{\omega_0 U} = \frac{\mid V \mid^2}{\omega_0 U}, \tag{3}$$

Using the simulation code HFSS, we estimate the normalized shunt impedance for an arbitrary offset in the dipole mode field. The so-determined normalized shunt impedance values for the dipole mode are listed in Table III. Table III shows the linearity of the output voltage of the low-Q IPBPM. Because R/Q is proportional to the square of the offset, the output voltage will be proportional to the root of R/Q. Therefore, the R/Q value at an offset of 2 mm should be larger than four times the R/Q value at 1 mm.

TABLE III
NORMALIZED SHUNT IMPEDANCE FOR DIPOLE MODES.

Offset (mm)	x-dipole mode (Ω)	y-dipole mode (Ω)
1	0.504	1.440
1.5	1.133	3.259
2	2.011	5.887

By using the R/Q factor of the low-Q IPBPM and the beam parameters of ATF2, we can fully evaluate the output voltage described by Eq. 4.

$$V_{out,0} = \frac{\omega q}{2} \sqrt{\frac{Z}{Q_{ext}} (R/Q)} \exp\left(-\frac{\omega^2 \sigma_z^2}{2c^2}\right). \tag{4}$$

The calculated position signals for an offset of 2 nm are approximately 7 and 12.5 μV for the x and y offsets, respectively. The low-Q IPBPM output sensitivity calculated using simulation results is larger than the previously recorded high-Q IPBPM output sensitivities. The main reason for the improvement in the output sensitivity is that, even though the Q_0 of both BPMs are similar, the Q_{ext} of the low-Q IPBPM is smaller than that of the high-Q IPBPM [5], which difference causes the difference in the output sensitivities between the two BPM models.

Figure 5(a) shows the simulated output signal in the waveguide port. The signal is jagged because it includes other modes coupled from the cavity to the waveguide, as well as the dipole mode. Through a fast Fourier transformation, the output signal is classified into modes in the frequency space, and the corresponding frequency spectra are shown in Fig. 6. A distinguishable peak is observed at ∼6.426 GHz, which is the design value for the y-dipole mode. In addition to the y-dipole mode, quadrupole and higher order dipole modes are also present. However, the common mode signals do not appear when the proposed design is used. In addition, an x-port and y-port isolation of -50 dB is achieved, as shown in Fig.6. By assuming a 3 GHz pass band, the signal is filtered (see Fig. 5(b)) and the signal decay time for the filtered signal is estimated to be ≈17 ns.

C. Fabrication and bench test

We fabricated a BPM block consisting of three copper parts for the rectangular sensor cavity, two pieces of stainless steel for the cylindrical reference cavity, subminiature version a (SMA) feedthroughs for signal pickup, and flanges for beam duct connection. The main difficulties in fabrication were the lack of a tuning pin and the irregular cavity surface. To realize frequency tuning without a tuning pin, we adjusted the cavity

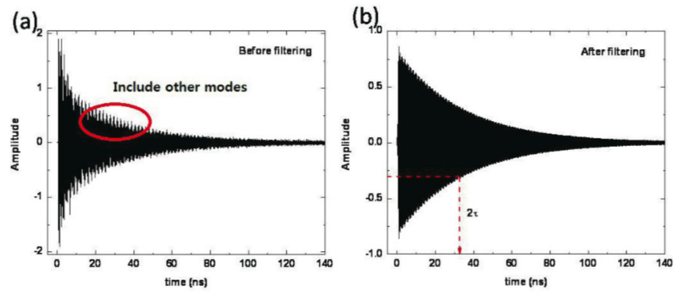

Fig. 5. Simulated output signals at the y port (a) before filtering and (b) after filtering. The band-pass filter eliminates the other mode signals from the 6.426 GHz y port signal. The simulated decay time is 17 ns after filtering.

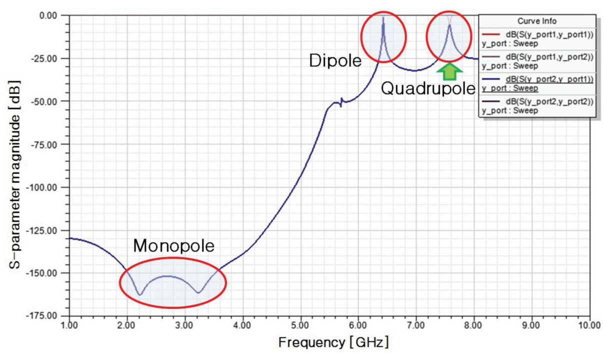

Fig. 6. Frequency spectra of the output signals for the y port obtained using HFSS.

dimensions to compensate for the frequency difference in the cold model. Because the external quality factor dominated over the loaded quality factor, that is, $Q_{ext} \ll Q_0$, ~5 μm the roughness of the cavity wall was treated.

TABLE IV
COMPARISON OF QUALITY FACTORS OF THE SIMULATION (SIM.) AND RF MEASUREMENT (MEAS.) RESULTS FOR THE FABRICATED BPM.

Port	Frequency (GHz)	Q_L	β	Q_0	Q_{ext}
Y (Sim.)	6.426	603	9	6020	670
Y (Meas.)	6.433	595.6	0.79	1066.2	1349.6

Table IV shows a comparison of the simulated quality factors and the measured quality factors of the y-port after the brazing. The measured external and internal quality factors show differences with respect to the simulation results. We assume that the reason for the difference between the simulated and measured results is the irregular surface machining. However, the measured Q_L was similar to the simulation result; thus, the expected output voltage was also similar to the simulation result.

Figure 7 shows the fabricated pieces of the low-Q BPM. The rectangular shape of the main cavity and the four wave guides were machined from the main copper piece from both ends. Four coupling slots were fabricated by electric discharge machining (EDM). For brazing the pieces, grooves were dug on the connection surfaces to insert wire fillers, and nickel was additionally plated on the stainless steel material surface.

Fig. 7. Fabricated pieces of the cavity. The sensor cavity is made by stacking three copper pieces and the reference cavity is made by stacking two stainless steel pieces.

Finally, the five pieces of copper and stainless steel were simultaneously brazed using Au filler.

TABLE V
RF SIMULATION (SIM.) SIGNAL PROPERTIES AND FABRICATED CAVITY MEASUREMENT (MEAS.) RESULTS.

Port	Frequency (GHz)	Bandwidth (MHz)	Decay time (ns)	Sensitivity
X (Sim.)	5.712	8.8	18	2.3 mV/μm/nC
X (Meas.)	5.716	7.1	22	1.7 mV/μm/nC
Y (Sim.)	6.426	10.7	15	3.9 mV/μm/nC
Y (Meas.)	6.433	10.8	15	3.4 mV/μm/nC
Ref. (Sim.)	6.426	5.5	29	3.27 V/nC
Ref. (Meas.)	6.429	4.2	38	3.47 V/nC

The properties of the completed cavities were verified through port-to-port measurements using a network analyzer. From the measurements of the resonance frequency of the dipole modes, coupling strength, and loaded quality factor, we extracted the basic parameters of the BPM signal with the calculated normalized shunt impedance along the beam offset. The RF test results are summarized in Table V along with the simulation results from HFSS.

III. BASIC BEAM TEST

After confirming the basic parameters using a network analyzer and investigating the contaminated signal through simulations, a basic beam test was performed for the low-Q cavity BPM, on the ATF beam line. The low-Q cavity BPM was installed in the last section of the extraction line at the ATF. The temperature was passively stabilized within 2 K variations per year and the ground vibrations were isolated within 4.3 nm at 40 Hz using a heavy granite table. More detailed temperature variations and ground variations are presented in the reference paper [5], [7], [9]. The layout of the last section of the extraction line is shown in Figs. 8.

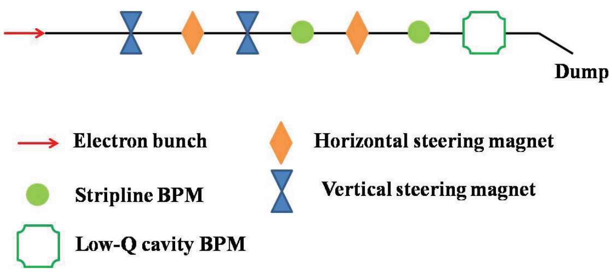

Fig. 8. Beam line layout of the last section of the ATF extraction line.

The layout of the basic electronics for the basic beam test are shown in Fig. 9. The overall sensitivity of the electronics was calibrated using a continuous wave (CW) signal source and a spectrum analyzer. The beam position was controlled with steering magnets and was monitored with strip-line BPMs. The beam positions monitored by the strip-line BPMs were extrapolated to determine the beam positions at the location of the cavity BPM. To simplify the beam optics, the quadrupole magnets in this region were turned off during the experiment.

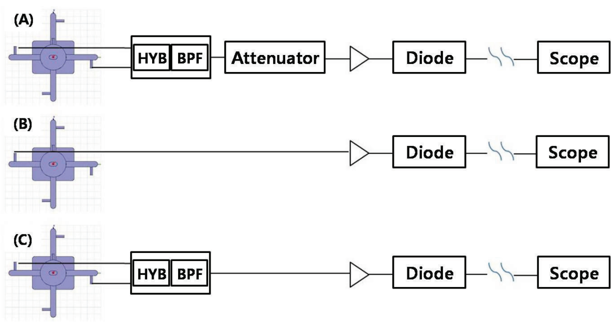

Fig. 9. Layout of the basic electronics used in the experiment. Detection electronics consisted of a 180° hybrid combiner with a band-pass filter, attenuator, amplifier, and diode. 9(a) layout are used 180° hybrid combiner with a band-pass filter, attenuator, amplifier, and diode. 9(b) layout are only used diode to measure the raw signal shape from cavity BPM. 9(c) layout are used 180° hybrid combiner with a band-pass filter, amplifier, and diode.

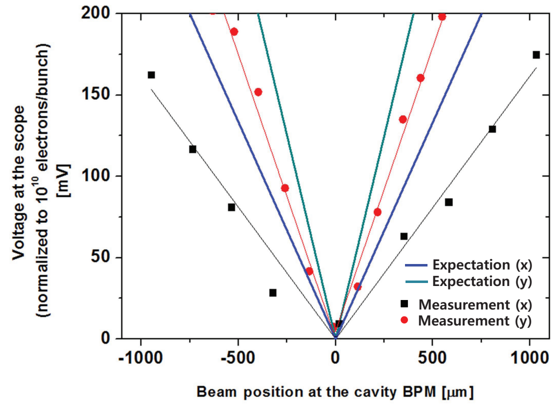

Fig. 10. Position sensitivity of the combined signal from two opposite ports of the cavity BPM. The data plot becomes V-shaped with its minimum at the electrical center of the cavity.

First, the beam position sensitivities for the x and y ports were measured to investigate the output signal from the cavity BPM. The beam orbit was controlled and changed using a pair of steering magnets (see Fig. 8). The combined signal from the two opposite ports of the BPM was detected using a simple electronics scheme, including an oscilloscope, as shown in Fig. 9(a). The peak voltage of the output signal was measured at different beam offset positions.

Figure 10 shows the measured peak voltage along the extrapolated orbit from the strip-line BPMs at the location of the cavity BPM. To confirm the result, the expected values based on simulation results were compared with the measured sensitivities of the low-Q cavity BPM. A difference of $\sim$4 dB was observed between the measured and expected voltages, which originated from the inaccurate electronics calibration. The electronics simulation indicates a 2 dB difference between the losses caused by the CW signal (used in electronics calibration) and the pulse signal (from the cavity BPM with the beam) at the diode. In addition, the inaccuracy of the spectrum analyzer used in the calibration was estimated as 3.25 dB [7]. Therefore, the difference of $\sim$4 dB is explained.

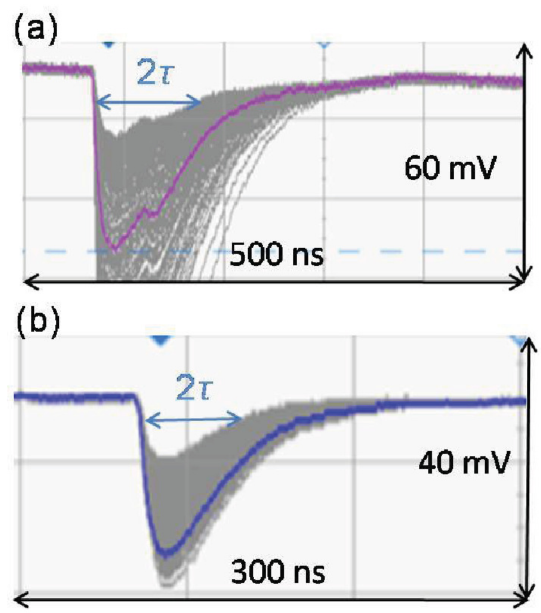

Fig. 11. Stacked waveforms of y dipole along the beam position jitter. (a) Layout in Fig. 9(b) and (b) layout in Fig. 9(c) are used.

The test for common mode contamination was performed by changing the beam orbit at the ATF beam line. As shown in Fig. 11, the common mode contamination can be roughly identified by stacking the waveforms of the signal along the change of the beam orbit. From the offset and decay time of the smallest offset waveform, the position signal and type of contamination source can be estimated roughly. In the absence of contamination of the signal, the smallest offset waveform should be zero; however, as shown in Fig. 11(a), the smallest offset waveforms had amplitudes of 20 mV for

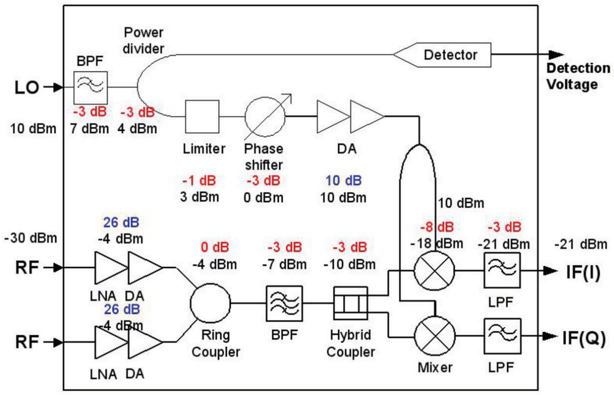

Fig. 13. Layout of the developed electronics system.

the y signal. Using the position sensitivity shown in Fig. 10, these amplitudes were converted to $\approx$3 μm for the y position. After the common mode signal was annihilated in the 180° hybrid combiner and its residual leak was cut off by the band-pass filter by using the layout in Fig. 9(c), the corresponding smallest offsets (in Fig. 11(b)) were also converted to $\approx$2.5 μm. Here 500 nm for the y position signals contaminated by the common mode were rejected by the 180° hybrid combiner with the band-pass filter. The remaining offsets, whose decay times were similar to that of the dipole mode in Fig. 11(b), could be explained by the cavity BPM tilt. From the simulation results, the remaining position offset signals were equivalent to $\sim$0.9 mrad for the y angle signal. Since both ends of the 15 cm long cavity BPM were aligned at the 1 mm level, the BPM could be tilted until $\sim$7 mrad. However, these remaining offset waveforms could be dramatically rejected by the phase filter.

In addition to the investigation of the signal separation between bunches, three bunch modes were also confirmed. The bunch-to-bunch time gap was $\sim$150 ns. The signals from the cavity BPM were well separated in Fig. 12 (left). A feedback study was performed using y-port signals, and Fig. 12 shows the beam feedback test results for the multibunch operation.

IV. ELECTRONICS

An electronics system was developed for processing the raw signals from the low-Q cavity BPM . A schematic diagram of the electronics is shown in Fig. 13.

The purpose of the electronics design is the reduction of the signal processing time for the fast beam feedback system. Therefore, we adopt single-stage homodyne electronics. Two output signals from the sensor cavity, with the same direction, are fed into a low-noise amplifier (LNA) and drive amplifier to increase the signal amplitude. The LNA is selected to reduce the noise figure (NF) of the entire electronics system. The noise figure of the electronics system is determined by the first part of the electronics; the relation can be explained by the following equations,

$$F_{total} = F_1 + \frac{F_2 - 1}{G_1} + \frac{F_3 - 1}{G_1 G_2} + ... + \frac{F_n - 1}{G_1 G_2 ... G_{n-1}}, \quad (5)$$

$$NF_{total} = 10\log_{10}\mathrm{F}_{\mathrm{total}}, \quad (6)$$

where the NF and gain of each module are F1, F2, ... , Fn and G1, G2, ... , Gn, respectively. Therefore, the NF of the entire system is determined by the NFs of the first elements of the electronics. The measured NF of the entire electronics system is 3.871 dB.

After signal amplification, the two RF signals are combined with an anti-phase hybrid. A band-pass filter (BPF) with a $\pm$200 MHz bandwidth is used after the two signals are combined, to reject other modes. To detect the IQ phase, the signal is split into two mixers and detected in a base band with orthogonal phases (I and Q). The bandwidth is determined by a 50 MHz low-pass filter (LPF) placed after the mixer. The longest signal processing time of the electronics is determined by this LPF. Because the LPF signal processing time is expected to be $\sim 1/\Delta f$, the entire electronics signal processing time is expected and measured to be $\sim$20ns.

The minimum detectable signal power of the entire system is measured as -83 dBm, which corresponds to 15.83 μV. The measured BPM output sensitivity under nominal beam conditions of the ATF is 5.44 μV/nm for the y-port. Therefore, the expected resolution limit of electronics is $\sim$3 nm. Additionally, the electronics is installed outside the tunnel and the long cable power loss is measured to be 8.5 dB; thus, the expected resolution with long cable power loss is $\sim$7.7 nm. The measurement results for the developed electronics module are listed in Table VI.

TABLE VI
ELECTRICAL SPECIFICATIONS OF THE ELECTRONICS.

Parameters	Units	Min.	Typ.	Max.
Frequency range	GHz	6.2	6.4	6.6
Output frequency	MHz	0		50
Conversion gain	dB	9.3	10.6	11.6
I, Q phase difference	degree	87	90	93
1-dB compression (input)	dBm	-15	-13	
Electronics NF at 10 MHz	dB		3.871	

V. POSITION RESOLUTION MEASUREMENT TEST SCHEME

The low-Q cavity BPM was installed at the extraction beam line of ATF2 to test the beam position resolution. Figure 14 shows one block of the developed low-Q cavity BPM and two high-Q cavity BPMs [7]. Two sets of horizontal movers and vertical movers were installed to align the beam center of each BPM. The electronic systems for the low-Q and high-Q cavity BPMs were used to convert the raw signal to the I–Q signal and were installed on the outside tunnel. The sensor cavity monitor was used to measure the beam position by using the dipole mode, while the reference cavity was used to measure the beam charge by using the monopole mode of the same resonant frequency as that of the sensor cavity. The output signal from the sensor cavity was fed into the electronics. We acquired I and Q signals after phase tuning using a phase shifter, in which the signals differed in phase by 90°. Band-pass filters were used to prevent the unwanted dipole modes in the signals. Additionlly, the low-Q cavity BPM was developed

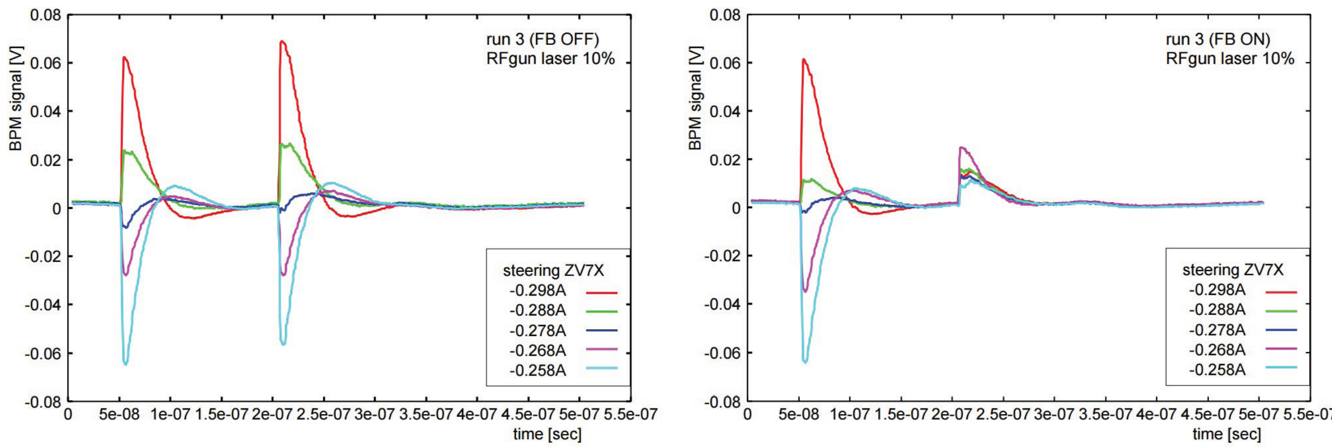

Fig. 12. Beam feedback test for multibunch beam operation. The time gap between bunches is ∼150 ns.

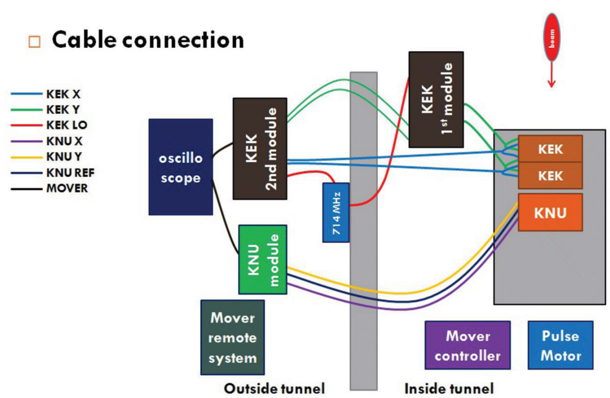

Fig. 14. Testing scheme for beam position resolution measurement of low-Q BPM.

to measure the orbit resolution in the vertical direction because horizontal beam size is very larger than vertical beam size. It means that a measurement of vertical orbit needs a magnitude of smaller orbit resolution. Therefore, beam test in vertical direction was performed to measure the y-port resolution. By this reason, we only used the y-port electronics and measured vertical beam position resolution. The orbit feedback system is also used for the y-port beam.

VI. Measurement of Beam Position Resolution

The position resolution of the low-Q BPM in the vertical direction was measured at ATF2. This measurement was performed in three steps: 1. I–Q tuning by using the phase shifter, 2. calibration to obtain the calibration factor, and 3. data collection for analyzing the beam position resolution of the low-Q BPM.

A. Basic idea

We used three BPMs to measure the beam position resolution of the low-Q cavity BPM. Because two BPMs were used to find the predicted position, the beam position resolution was defined by "the RMS of the residual between the measured and predicted beam positions of the low-Q cavity BPM" × "geometrical factor." The predicted beam position was calculated from the two high-Q cavity BPMs, and the geometrical factor was used to compensate for the propagation of error caused by the alignments of the three cavity BPMs used to calculate the resolution of a single cavity, assuming that the three cavities have the same position resolution. Even though we assumed that the three BPMs have the same position resolution, the low-Q IPBPM could not achieve a resolution below the position resolution of the high-Q IPBPM because the predicted position of the low-Q IPBPM was calculated using the two high-Q IPBPMs.

B. I–Q tuning

I–Q tuning was performed using an oscilloscope to reduce the effect of noise on the position signal. When the maximum value of the I signal was reached, the Q signal was set to the zero position using the phase shifter. In this setting, the I and Q signals represent the beam position and beam trajectory angle signals, respectively. If I–Q tuning is not performed, the electronics can easily become saturated by the large beam trajectory angle and a correct beam position resolution cannot be expected.

C. Calibration procedure

The calibration run was performed to calibrate the signal from the sensor cavity with respect to the actual beam position. To monitor the response of the sensor cavities in the vertical direction, the beam was swept along the sensor cavities by vertical movers. An electron beam was swept against the sensor cavities by controlling the mover current, and the response of the sensor cavities was monitored. During the calibration run, the average beam charge was 0.2×10^{10} particles and the calibration was swept within a range of 40 μm.

The intermediate frequency (IF) parts of the low-Q IPBPM electronics were connected to 40 dB of extra amplification to achieve a higher calibration factor. However, the other high-Q IPBPM electronics did not need any amplifiers because the high-Q electronics already had sufficient system gain.

The calibration run was done three times to determine the calibration factors. The results of the calibration run for each cavity BPM are listed in Table VII.

TABLE VII
RESULTS OF THE CALIBRATION RUNS.

BPM type	Calibration factor (mV/nm)	Statistical error (mV/nm)
Low-Q BPM (w/40dB amp.)	0.674	0.0264
High-Q BPM 1	0.922	0.0451
High-Q BPM 2	0.720	0.0260

D. Position resolution study

The position resolution (σ) of the low-Q cavity BPM was estimated with a fixed beam orbiting near the beam center. The electronic setup was the same as in the calibration run. The main purpose of this run was to measure the residual (Δ), which was the difference between the measured position obtained using the low-Q BPM ($Y_{I_{meas}}$) and the extrapolated position at the location of the low-Q cavity BPM obtained using the high-Q BPM ($Y_{I_{ext}}$). The residual is calculated as follows:

$$\Delta = Y_{I_{meas}} - Y_{I_{ext}}. \tag{7}$$

Figures 15 and 16 show the results of this run for 500 events. The RMS of the residual was estimated as 440 nm during a 500-event resolution run, which value was divided by the calibration factor, already. To obtain the beam position resolution of a single cavity, we need to consider the geometrical factor (GF), which is a coefficient determined by the geometrical configurations of the three cavities. The GF of these three BPMs was calculated to be ≈0.8. Therefore, the beam position resolution was given by

$$\text{resolution} = \text{GF} \times \frac{\text{RMS of residual}}{\text{calibration factor}}. \tag{8}$$

The position resolution of the low-Q cavity BPM was measured as 352 nm when we collected these data with an average beam charge of 0.2×10^{10} particles.

When we converted the position resolution with the nominal beam charge of ATF2, which is 10^{10} particles, the position resolution of the low-Q cavity BPM was expected to be ~70 nm. In this study, we did not utilize the position information from the x ports of the three BPMs fully. Furthermore, the minimal mover step size was ~1 μm; this mover step accuracy caused a large error bar for the calibration factor. Therefore, we performed several calibration runs to obtain more precise calibration factors, and if we could improve the mover accuracy, more accurate calibration factors could be measured and the beam position could be predicted precisely. If we use the full information for both the x- and y-port signals from the three BPMs, we would be able to achieve a position resolution less than 70 nm.

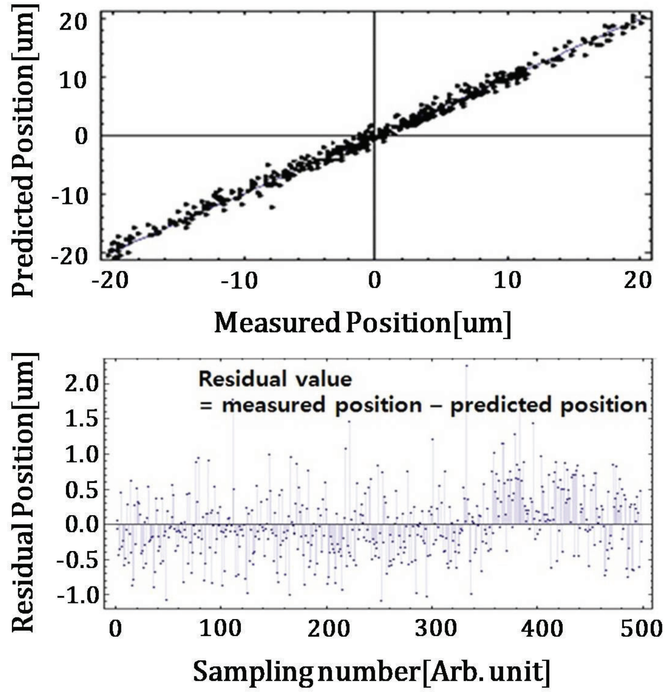

Fig. 15. Measured position versus predicted position (top). Residual position from 500 events (bottom).

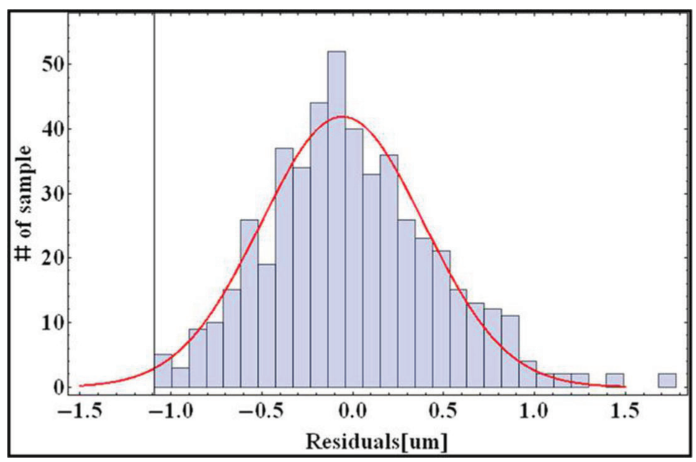

Fig. 16. Gaussian fitting of residual position.

VII. CONCLUSION

In this paper we described the development of a low-Q cavity BPM consisting of a one-cell sensor cavity and a one-cell reference cavity. The proposed BPM had a structure similar to that of the high-Q cavity BPM developed by KEK, but exhibited a short decay time with clear residual leakage for fast orbit feedback control with 150 ns bunch spacing. The characteristics of the cavity BPM were examined by performing a beam test. Contaminated common mode signals, which were equivalent to ~2 μm and ~500 nm for the x and y position signals, respectively, were confirmed to have been rejected by a commercial band-pass filter and a 180° hybrid circuit. The signals from the sensor cavity were well separated in a three-bunch operation, in which a bunch spacing of 150 ns was observed due to the decay times of 22, 15, and 38 ns for the x, y, and intensity signals, respectively. The analog electronics for the signal processing within 20 ns were also developed. The beam position resolution test was also performed at ATF2. The measured beam position resolution was 352 nm for 0.2×10^{10} particles and the expected resolution for a nominal beam charge of 10^{10} particles was 70 nm in the vertical direction. Further improvements in the electronics to achieve better position resolution are under consideration, and more beam tests will be performed.

ACKNOWLEDGMENTS

The authors wish to express their gratitude to all operators and support staff of the ATF group. This research was supported by Korea University Grant.

REFERENCES

[1] T. Behnke, J. E. Brau, B. Foster, J. Fuster, M. Harrison, et al., "The International Linear Collider Technical De- sign Report - Volume 1: Executive Summary", 2013. [Online]. Available: physics.acc-ph, arXiv:1306.6327. Accessed on: June 3, 2017.
[2] P. N. Burrows et al. "The FONT4 ILC Intra-train Beam-based Digital Feedback System Prototype" in Proc. PAC2007, Albuquerque, New Mexico, 2007, pp. 416-418.
[3] T. Shintake, Development of Nanometer Resolution RF-BPMs, in Proc. HEACC 98, Dubna, Russia, 1998, p.341-345.
[4] P. Bambade et al. Present status and first results of the final focus beam line at the KEK Accelerator Test Facility, Phys. Rev. ST Accel. Beams, vol 13, Art. no. 042801, Apr. 2010.
[5] Y. Inoue et al., "Development of a high-resolution cavity-beam position monitor", Phys. Rev. ST Accel. Beams, vol 11, Art. no. 062801, 2008.
[6] Z. Li et al, Cavity BPM with dipole-mode selective coupler, in Proc. PAC2003, Portland, OR, 2003, Art. no. ROAB004.
[7] T. Nakamura, "Development of Beam-position Monitors with High Position Resolution", M.S. thesis, Department of Physics, The University of Tokyo, Tokyo, 2008.
[8] HFSS. ANSYS. [Online]. Available: http://www.ansys.com. Accessed on: June 3, 2017.
[9] H. Yamaoka, Private communication. Apr. 2004. [Online]. Available: http://acfahep.kek.jp/subg/ir/nanoBPM/transparency/040428/yamaoka.pdf